GROUND PENETRATING RADAR LOCATION OF BURIED AVALANCHE VICTIMS

Justin Modroo and Gary R. Olhoeft
jmodroo@mines.edu – golhoeft@mines.edu
Colorado School of Mines - Department of Geophysics
1500 Illinois St., Golden, CO 80401

ABSTRACT:

The best way to survive being buried alive in an avalanche is with the use of requisite signal locator tools such as a personal transceiver or a RECCO reflector. If a person is buried without this equipment, search and rescue crews are limited to using rescue dogs or a probe line to locate the victim. Most of these methods have problems, including the RECCO system. Because of these problems, some victims are not recovered until the spring thaw. It is obvious that a better rescue/recovery method is needed. Ground penetrating radar (GPR) is an electromagnetic geophysical tool used extensively to image and characterize the subsurface. GPR could be applied as an imaging tool to locate and rescue/recover a buried avalanche victim. An avalanche burial simulation test was conducted at the Loveland Ski Area, CO. The test provided time lapse GPR reflection data for a buried human body mass equivalent (BME) as the core temperature dropped from 38°C to 0°C in 110 hours. The test also produced GPR reflection signatures of natural and man-made objects associated with avalanche debris. By comparing GPR wavelet traces of each target, the GPR data were used to distinguish between the BME, man-made objects, and natural objects. The experiment also proved that a 900 MHz antenna can uniquely identify a buried avalanche victim once a 2 cm air pocket has melted around the body. This experiment proved that GPR can be used to image and locate a buried avalanche victim. Hopefully in the future, this technology will be able to save human lives.

KEYWORDS: (GPR, rescue, avalanche, imaging, location, recovery).

1. GROUND PENETRATING RADAR

1.1 *GPR history*

Ground Penetrating Radar (GPR) is a non-invasive electromagnetic geophysical tool that is used to produce pseudo cross-section images of the subsurface. When GPR data is collected along a 2D profile, it provides laterally spaced traces detailing the reflected energy from within the subsurface. By utilizing and fully understanding the GPR system (and associated consequences), physical properties of the subsurface can be interpreted to produce a more realistic cross-section.

GPR was first used to help characterize and study glaciers over 75 years ago. The very first published GPR survey was used to determine the depth of a glacier, reported in 1929 (Stern, 1929). The technology resurfaced in the 1950's when planes began crashing into the Greenland ice sheet. The planes crashed due to false radar altimeter readings. The radar altimeter failed due to a lack of reflected energy from the air-ice boundary, and calculated a false altitude using the ice-ground boundary. This spawned a large increase of GPR to image glaciers and ice sheets. Since then, the number of applications for GPR has grown significantly along with the information and knowledge gained from the data (Olhoeft, 1988).

Current uses of GPR range from simple utility detection to complex monitoring of underground environmental spills. Archaeologists use GPR for non-invasive subsurface site investigation; farmers are using GPR to map water content to design more efficient watering systems and to predict crop yield. GPR has been successfully used to map water tables, locate land mines and un-exploded ordnance, measure the quality and thickness of concrete structures, and many other useful applications.

It should be possible to effectively image a human body buried in snow utilizing GPR (Niessen 1994, Yamaguchi 1991). It is widely known that snow and ice provide an excellent propagation media for GPR waves (Achammer and Denoth 1994). In snow, a human body (composed of mostly liquid and is highly conductive) serves as a high contrast reflector for GPR waves (Olhoeft 1998). An unfrozen human body buried in snow is an ideal GPR target. This phenomenon occurs due to changing dielectric properties of water, and the conduction properties of the human body. If successful, GPR could be a potential life saving application for avalanche victims.

1.2 *GPR theory*

GPR utilizes electromagnetic (EM) wave propagation through the subsurface at frequencies ranging from megahertz (MHz) to gigahertz (GHz). An antenna (equipped with a transmitter and receiver) is used to generate an EM pulse that propagates through the subsurface. Some of the propagating EM energy will be scattered (reflected) when it encounters a medium with contrasting electrical or magnetic properties. The reflected energy is measured by the receiver and is then sent to a computer to be saved and displayed in real-time. By moving the antenna along a 2D profile, lateral traces are grouped together to provide a cross-section like image of the subsurface. By understanding the interactions between the electric and magnetic fields and charged particles, the subsurface material can be characterized correctly leading to a true cross-section image.

Charge motion (current) is created from external forces, such as resulted from an electric field or a time varying magnetic field (Olhoeft 1998). The change in charge velocity (acceleration) results in electromagnetic radiation. Maxwell's equations describe the interaction between electric and magnetic fields and the corresponding coupled process propagating as a three-dimensional, polarized, vector wave field, known as electromagnetic radiation (Balanis 1989).

The propagation of EM waves in the subsurface is described with the complex radar equation (Annan 2001 and Powers 1997). Variables influencing the radar equation include: antenna properties, geometry, target size, shape, and orientation, and contrast in physical properties between the target and the surrounding host medium (relative dielectric permittivity (ε_r), magnetic permeability, and conductivity (σ)).

Table 1.1 shows the relative dielectric permittivity and conductivity for some relevant materials. For a complete list of various body parts and their corresponding electrical properties see Gabriel and Gabriel (1996). The electrical properties of different materials are from Annan (2001). The magnetic permeability of relevant materials is assumed to be that of free space and will henceforth be neglected.

Material	ε_r	σ (mS/m)
Snow	2 to 12	0.00
Ice	3 to 4	0.01
Air	1.0	0.00
Fresh water	80.0	0.03
Rock	5 to 10	.01 to 2
Wood	8 to 15	0.02
Body	50.0	800.00
Metal	∞	∞

Table 1.1 Electrical properties for relevant material associated with avalanche debris.

2. AVALANCHE BURIAL SIMULATION EXPERIMENT

2.1 *Procedure*

To help test the use of GPR as an avalanche rescue/recovery imaging system, the following fundamental questions need to be answered. How will GPR respond to a freezing body? How long will it take for a body to freeze while buried in snow? Will it be possible to distinguish a body from other anomalies found in avalanche debris?

To answer these questions, an experiment was designed to simulate the environment of an avalanche burial. A human body mass equivalent (BME) was buried in snow to simulate the buried victim. The BME's core temperature and GPR response were measured over time as the BME froze. Also, a database of GPR responses to natural and man-made objects was acquired. Loveland Ski Area (CO, USA) cooperated by providing a location for the test, where they consolidated snow from plowing their parking lot. The experiment took place from November 21-25, 2003.

In order to simulate the human body, the BME needed similar electrical and thermal

properties. Pigs have been used for xenotransplantation of organs into humans (Appel 2001, Wolf 1997) because they have similar physiological properties to the human body. A common Yorkshire cross swine was used in this experiment. The Yorkshire family is Suidae, the genus is Sus, and is known as the Sus Scofa species. Colorado State University's (CSU) regulations were followed regarding animal research in the absence of any at the Colorado School of Mines. In accordance with CSU's Animal Care and Use Committee (ACUC), a pig destined for slaughter was intercepted between auction and butcher. A veterinarian then euthanized the pig, an hour later, the experiment began with the burial of the pig in snow. The BME weighed approximately 145 pounds, was 1 meter long and 60 centimeters tall.

To measure the core temperature of the BME, a specially designed thermometer pill (CorTemp technology HQ Inc. Palmetto, FL) was made for the BME to swallow prior to euthanization. The pill contains an oscillating crystal sensitive to temperature. The pill transmits the crystal's signal to a nearby receiving unit operating at 252 KHz.

On Friday, November 21st, the BME was legally purchased and euthanized by a veterinarian. The BME was buried in the deepest part of the snow pile. There was 0.9 meter (3 feet) of snow under the BME and roughly 0.76 meter (2.5 feet) above it. The BME was placed on its side with the GPR traverse orientated along the long axis of the body. Once buried, a GPR test line was created directly above the BME. Figure 2.1 shows a photo of the survey line. The beginning of line (BOL) and end of line (EOL) are annotated along with the corresponding target burial locations, and a person for scale.

A Sensors and Software Pulse-Ekko 1000 GPR unit was used to acquire the data using two different ground coupled antennas: 900 MHz and 450 MHz. Most GPR measurements were collected using the 900 MHz antenna, and the 450 MHz antenna was used less frequently.

The first measurements were gathered at 110 minutes (900 MHz) and 121 minutes (450 MHz) after burial. The data were collected using a 30 nanosecond time window, in continuous mode with one stack. The test line consisted of fiducial markers every three feet to ensure accuracy of the survey geometry. A track having the width of the GPR antennas was made to ensure that the same line was mapped with each repetition, and to achieve maximum coupling between the antenna

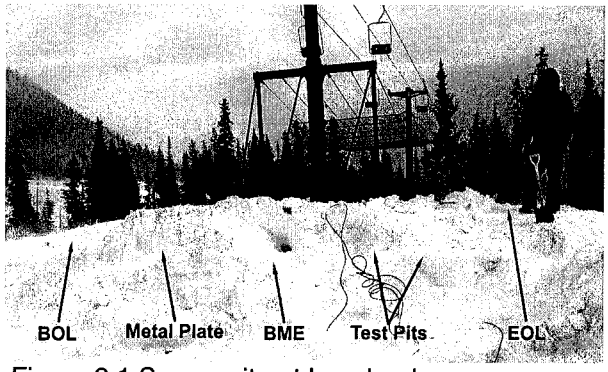

Figure 2.1 Survey site at Loveland.

and snow. A metal plate was buried near the BOL for calibration purposes. Two different test pits were located near the EOL, which hosted several different natural and man-made objects.

For the first 16 hours, a GPR measurement was made every half hour. The GPR measurement rate was then changed to one every hour. Problems did arise and staying consistent on the hour proved almost impossible due to blown fuses, cold and damp equipment (during a blizzard), and cold batteries (at night).

2.2 *Data*

Four temperature measurements were recorded during the experiment: the BME's core, the air, the surface snow, and ambient snow. The CorTemp thermometer pill worked well, providing a large amount of data. The BME's core temperature started out at approximately 38° C (close to the human normal 37° C), exponentially declining over 110 hours to 0° C freezing, with the ambient snow temperature at a relatively constant -6° C. Figure 2.2 shows four different temperature measurements for the first 45 hours of the experiment. During the first quarter of the experiment the air temperature dropped below -20° C. It should be noted that the surface snow temperature did reflect the changing air temperature, while the ambient snow temperature did not. The gaps in the data are due to mandatory absence from the experiment site.

Some figures will contain a label with the frequency and numbers representing the elapsed time since the BME's burial in the following format (h:mm). Figure 2.3 shows the comparison between the first GPR lines collected using each frequency, at which time the BME's core temperature was 37° C. In this early phase of the experiment, three targets are easily distinguishable with both frequencies. These

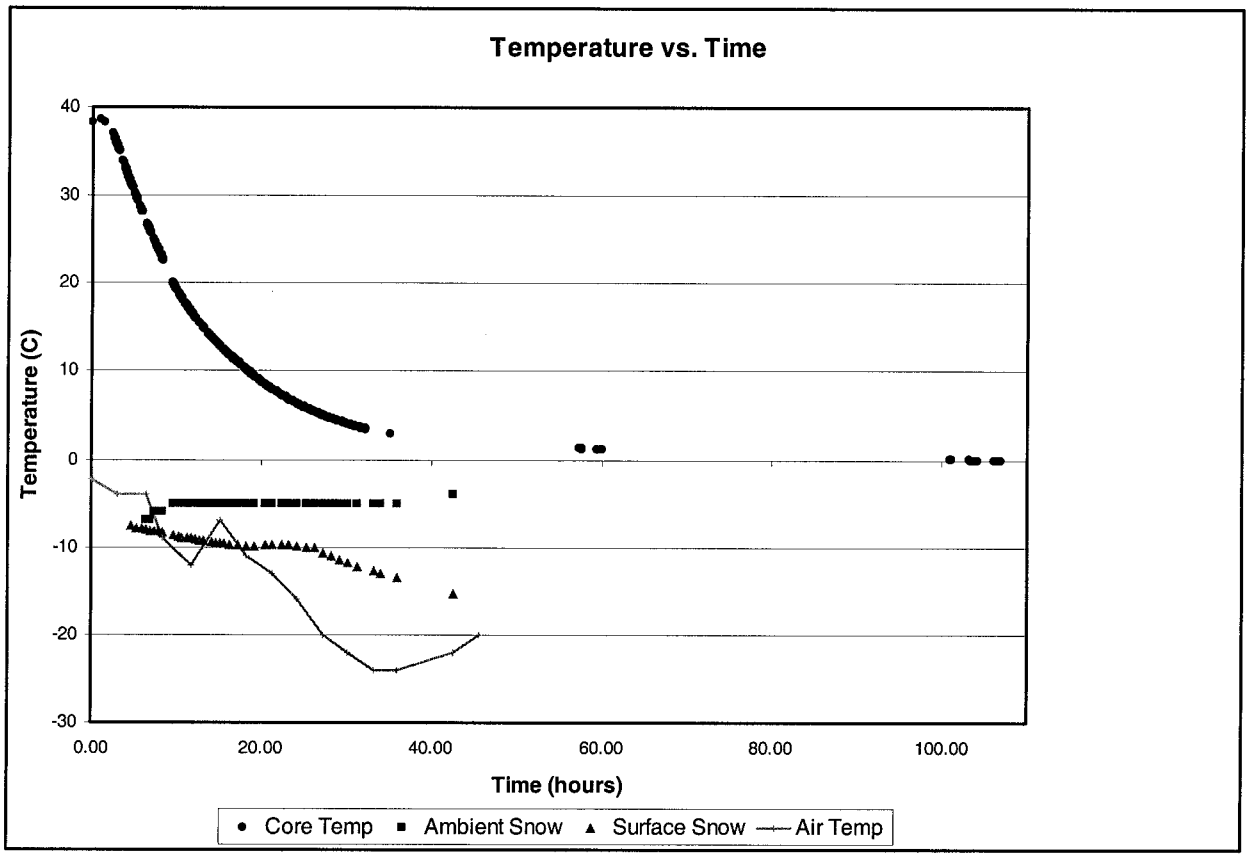

Figure 2.2 Temperature data for the experiment.

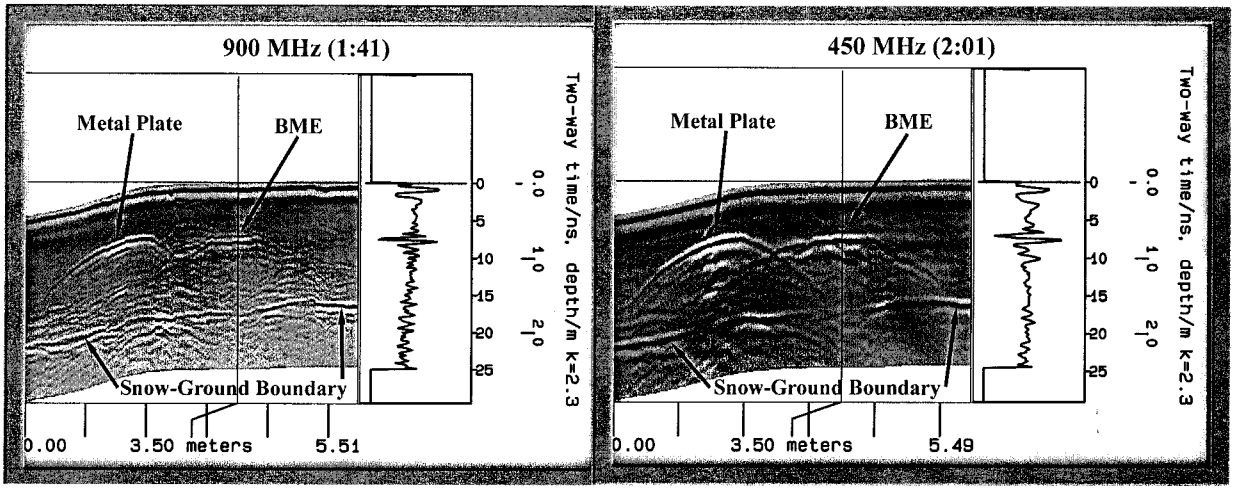

Figure 2.3 GPR data comparison between the earliest 900 MHz and 450 MHz data. Where (1:41) represents one hour and forty-one minutes after burial, etc. The x-axis is the distance traversed in meters. The y-axis is the two way travel time in nanoseconds, and also depth in meters (with the dielectric permittivity equal to 2.3). The solid vertical line through the BME target at 3.5 m traverse is a single wiggle trace, plotted to the right of the data and left of the y-axis values. The data have been corrected for topography.

targets are the metal plate, the BME, and the snow/ground boundary, annotated in figure 2.3.

All three targets are easily mapped with both antennas, which is proof that both frequencies have sufficient penetration and resolution to image the target for this experiment. It is easy to see how the 900 MHz provides better resolution than the 450 MHz data. The BME's GPR response (across the long axis of the body) is the summation of several reflections from different parts of the body. These main reflectors produced several hyperbolas that merge together in the data. This grouping of reflections and recorded responses could be a unique geometric signature used to detect a body relative to other avalanche debris.

Figure 2.4 shows three different 450 MHz lines. Notice that the BME is recognizable in each GPR line, even with a core temperature of 0º C. Now, focus on the natural and man-made objects buried in the test pits near the EOL. The top GPR line (14:22) has two rocks and two dirt clods buried in the test pits. The middle GPR line (43:10) has a ski pole and a ski buried in the test pits. The bottom line (94:15) has a freshly cut log and the pine tree buried in the test pits. Notice that the rocks and dirt clods look relatively faint, while all the man-made targets, the BME, and the wood are easily recognizable. To help provide a interpretation of the data, full waveform analysis was performed.

GRORADAR software was used to pick the normal incident trace of a GPR reflection for the various targets, which was output as a binary file and then analyzed using Matlab software. Figure 2.5 shows the trace of a normal incident GPR reflection from the BME.

This is an example of what the traces look like, with the target wavelet in bold. All of the trace amplitudes were normalized to the largest value of the direct arrival, displaying the measurement as "relative amplitude". The relative amplitude represents the amount of reflected energy from the target, where the metal plate is a perfect reflector (reflecting 100% of the energy). For future reference, when discussing the wavelet shape and amplitude, only the target wavelet will be shown.

Figure 2.6 shows several 900 MHz target wavelets that have been picked out of each trace for easier viewing. The targets include three different BME wavelets, natural, and man-made objects. The BME reflection has the largest relative amplitude (50%-32%), excluding the metal plate. As the BME froze, the amplitude did decrease as represented by the later time BME wavelets. The snow / ground boundary has the next largest relative amplitude (39%). This large reflector is helpful because it sets a distinguishable boundary to aid in the interpretation process. The later BME wavelets amplitudes are relatively similar to man-made objects with metal, like the ski, ski pole, and ski boot (36%-29%). The smallest reflections were from the natural objects and the plastic helmet (26%-12%). Notice the wood and rock amplitudes are smaller than all of the BME's amplitudes.

The next observation from figure 2.6 is that the BME wavelet has a unique shape relative to all the other target wavelets. The metal plate emphasizes the "typical" wavelet with two negative peaks and only one positive peak. Where, the BME has a "unique" wavelet that has two positive peaks and one negative peak. The reason for this unique shape will be explained in the modeling section.

Figure 2.7 has nine 450 MHz BME wavelets taken during different time ranging from 2 hours to 94 hours after burial. There are three main observation as to how the wavelet evolves as the core temperature drops. In the first two graphs the first positive peak is smaller than the second positive peak, where in all the other graphs they are of similar size. Secondly, the amplitude starts out rapidly increasing (34%), where at about 8 hours after burial the wavelet reaches a maximum (50%) and then slowly decreases over the next 102 hours(34%). The earliest and latest measurements have approximately the same size.

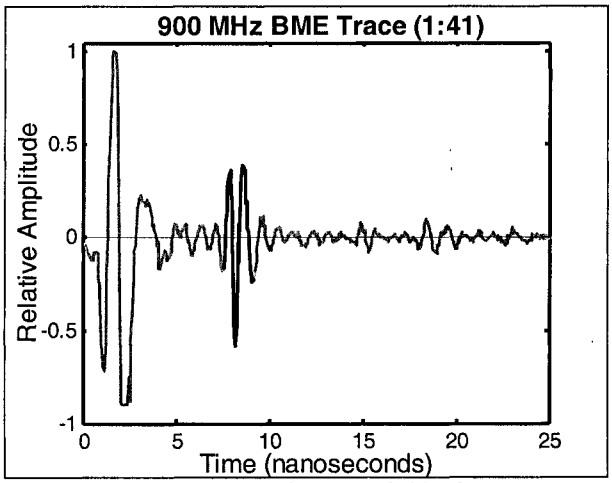

Figure 2.5 BME trace for 900 MHz frequency to show wavelet selection.

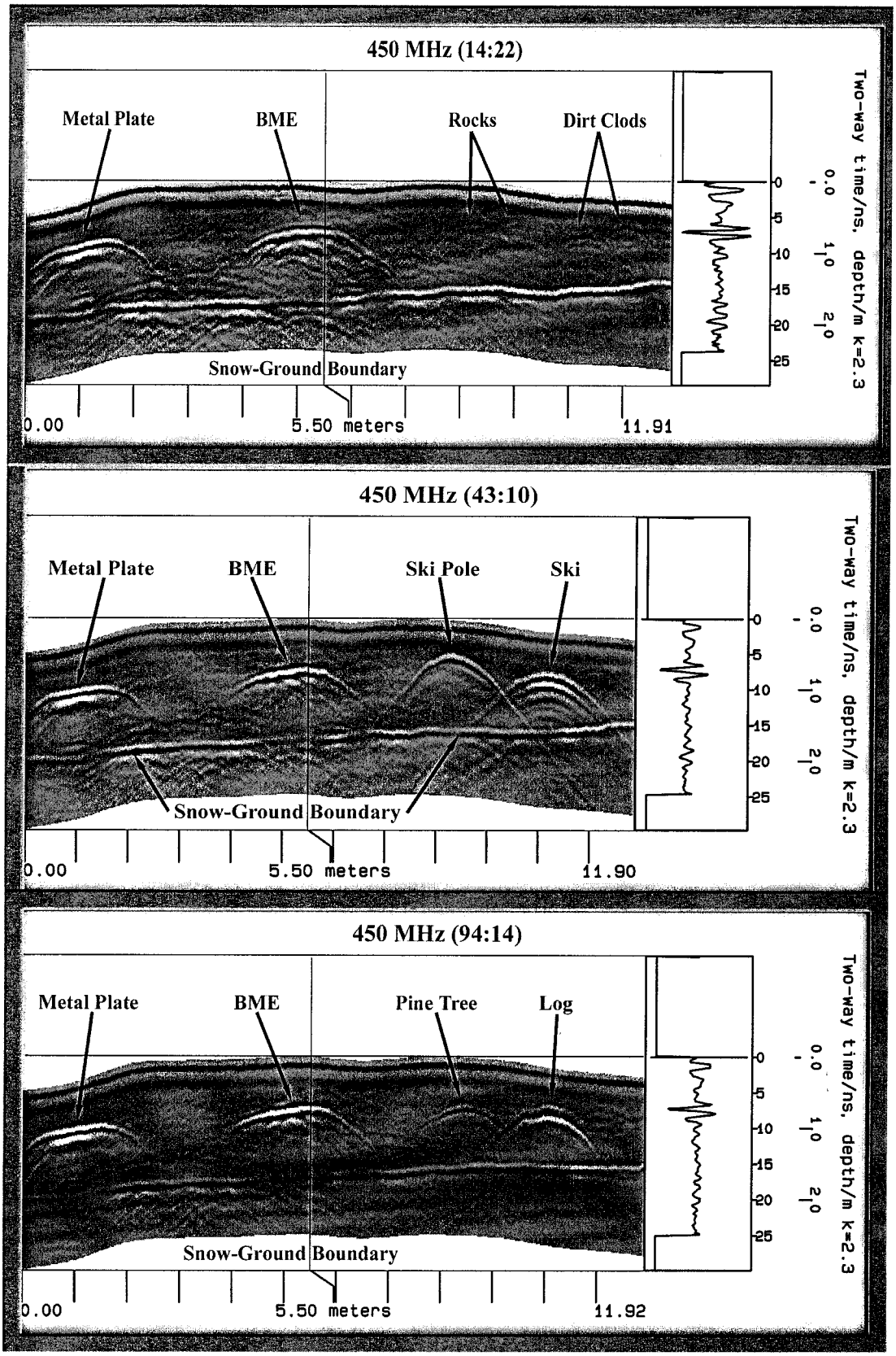

Figure 2.4 Three different 450 MHz GPR measurements at different times during the experiment.

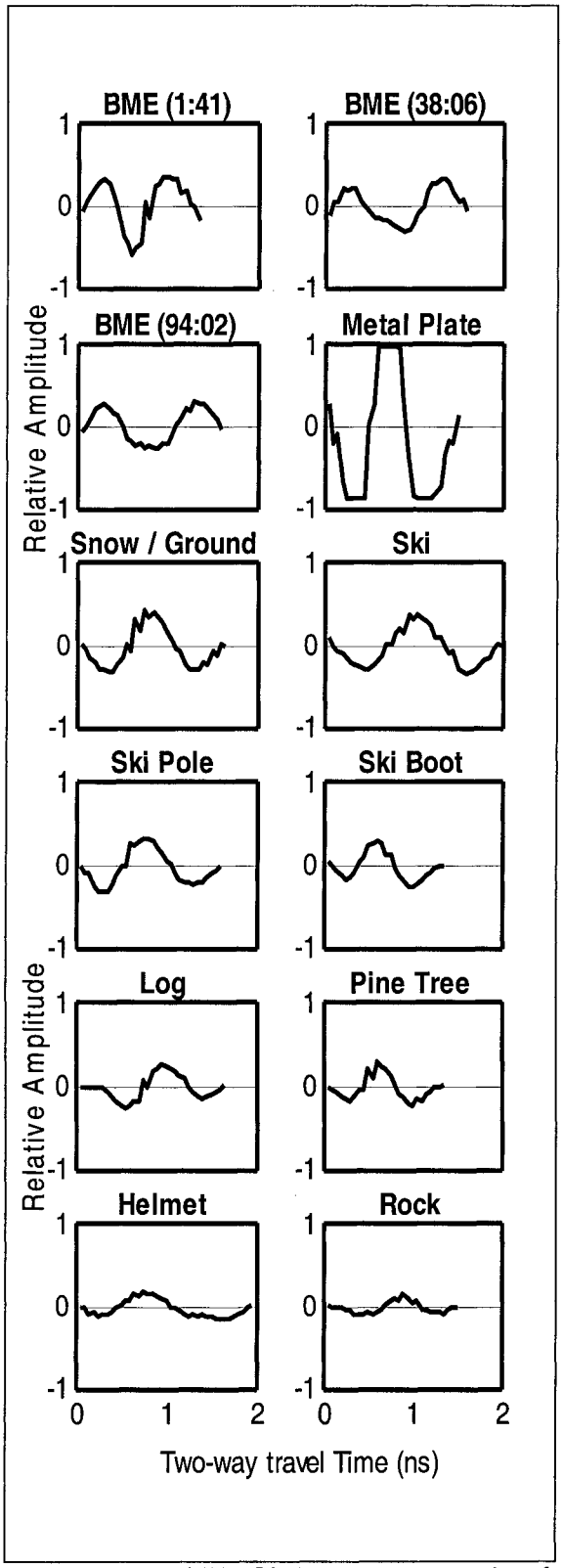

Figure 2.6 900 MHz GPR response wavelets from different targets.

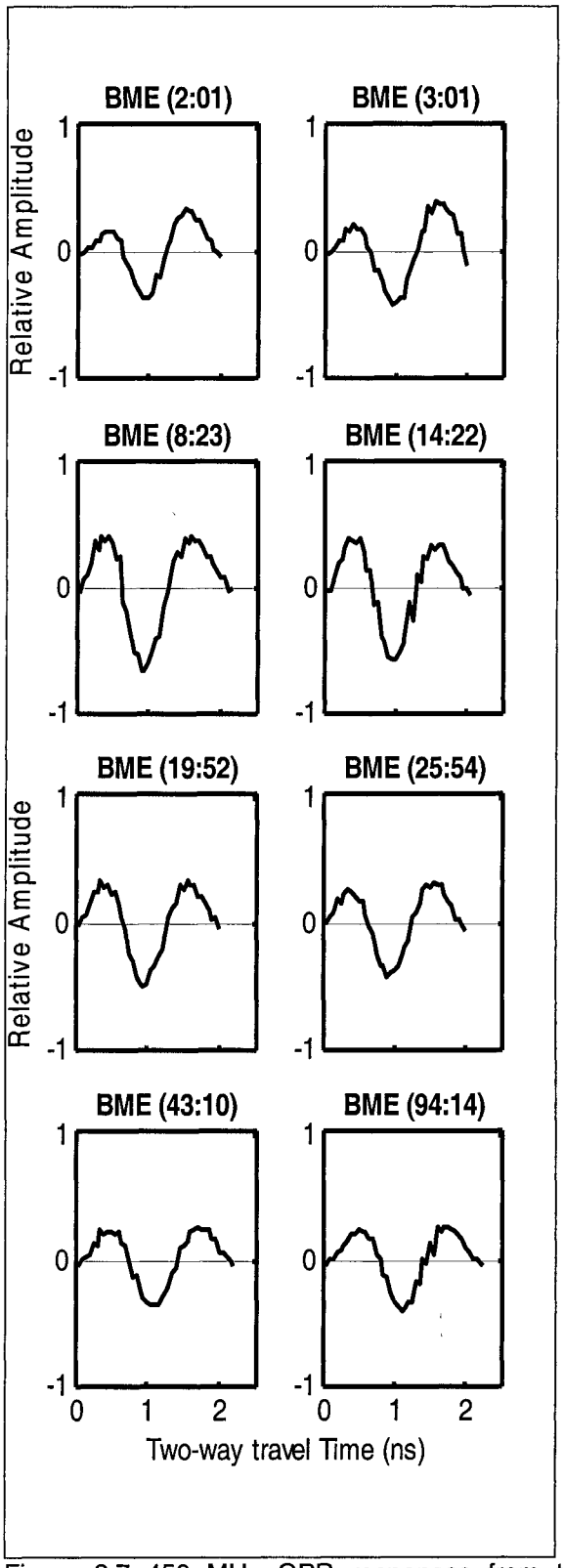

Figure 2.7 450 MHz GPR responses from the BME at different times.

2.3 Modeling

Full wave-form modeling was performed using the GRORADAR software. This is a convolution model that uses medium properties to physically model the behavior of an EM pulse traveling through different layers. Some assumptions of the model are: the EM wave is in the far field, and the layers are flat and horizontal and also smooth relative to a wavelength (Duke, 1990). Table 2.1 provides the input parameters for each of the six layers used in the model, including thickness, electrical conductivity, and the relative dielectric permittivity. The ice, air, and frozen skin layer thickness are labeled with an X. These were the variables changing during the modeling. Each one of these three layers were incremented with a uniform thickness. Figure 2.8 shows a drawing of what the layered model looks like.

Figure 2.9 shows the modeled response for the 450 MHz frequency. The first, top to bottom, shows the response from three layers, a human body with snow above and below (the ice, air, and frozen skin layer thickness is equal to 0). The final six models introduce three new layers (ice, air, and frozen skin) that are located above the human body and below the snow. This was used to model an "air gap" that develops above the victim's body as body heat melts surrounding snow. These new layers are all incremented with a thickness of X. Each new model was given a 1 cm increment. So, in the final model, each new layer has a thickness of 6 cm.

As the thickness of the "air gap" increased, the thin layer sequence provided constructive and destructive interference that completely changed the shape of the wavelet from "typical" to "unique". The X = 4 cm model is a similar match to the shape of the earliest 450 MHz BME reflected wavelet (2:01). The modeling did agree with both the 900 MHz and 450 MHz data, in which a 4 cm air pocket had developed after 2 hours of burial.

Layer	Thickness (m)	σ	ε_r
1. Snow	1.0	0	2.3
2. Ice	X	0.01	4
3. Air	X	0	1
4. Frozen Skin	X	800	30
5. Body		800	50
6. Snow	Infinite	0	2.3

Table 2.1 Input parameters for full waveform model (σ is measured in mS/m).

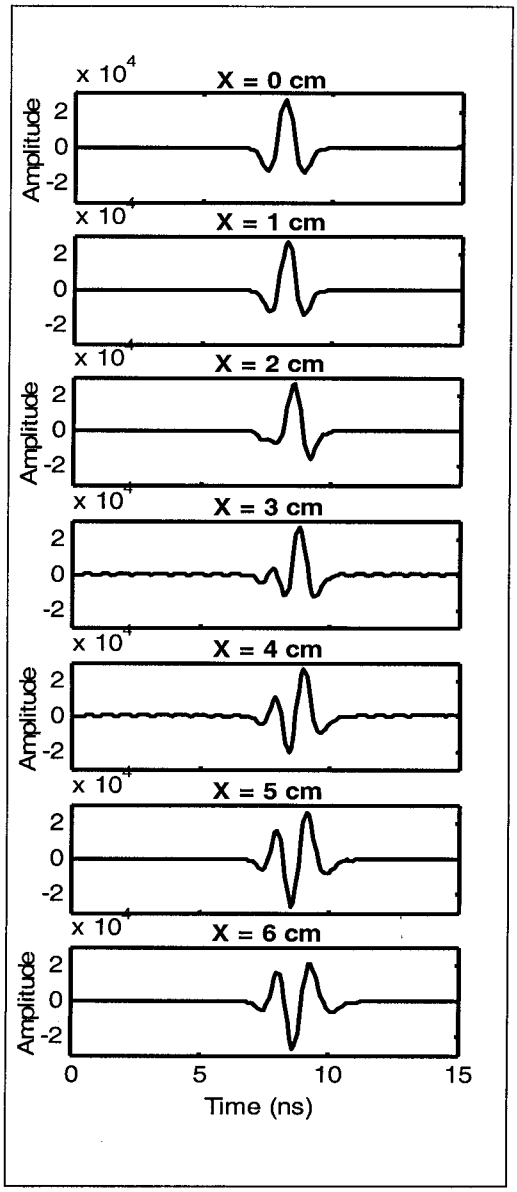

Figure 2.9 450 MHz six layer model response for varying thickness of ice, air, and frozen skin layers.

3. CONCLUSION

After analyzing the experiment data we learned: 1) the 145 pound BME completely froze (from 38° C to 0° C) over 110 hours while buried in snow with an ambient temperature of -7° C. 2) GPR can effectively locate the BME regardless of core temperature. Figure 2-10 plots the 900 MHz BME reflection wavelet negative amplitude minima that has been normalized to the temperature data. The wavelet amplitude increases during the first 8 hours, and then begins an exponential decline, that matches well with the temperature decline. The increasing amplitude is caused from the evolution of the wavelet from "typical" to "unique". At the time of the maximum amplitude, the air pocked and thin layer sequence were completely resolvable with the 900 MHz frequency. 3) GPR can uniquely identify man-made objects from natural objects based solely on wavelet amplitude comparison. 4) the 900 MHz antenna is able to uniquely identify a body once a 2 cm air pocket (4 cm for the 450 MHz) and associated ice layers have developed by body heat melting of snow and refreezing to ice to produce a unique wavelet reflection signature, as a result of constructive and destructive interference in the thin layer sequence.

Currently, there is no user friendly software to help an inexperienced GPR user identify a buried avalanche victim. Locating a buried avalanche victim with GPR requires specialized experience, due to the many variables and the complexity of the problem. Antenna coupling with avalanche debris will also pose a problem, if typical ground coupled antennas are used.

This experiment proved that GPR will be able to locate, image and identify a buried avalanche victim's body while still alive and after freezing. This opens the door for a prototype to be designed and implemented for search and rescue crews. The best and most efficient way to map avalanche debris with GPR would be with the use of a helicopter, due to avalanche site access problems and needed response speed. The helicopter could be mounted with a GPR antenna array and be used to map the avalanche debris, locate a positive anomaly, and deploy rescuers. The other option is to have a portable unit that a skier could use to search avalanche debris, similar to a how a transceiver search is performed.

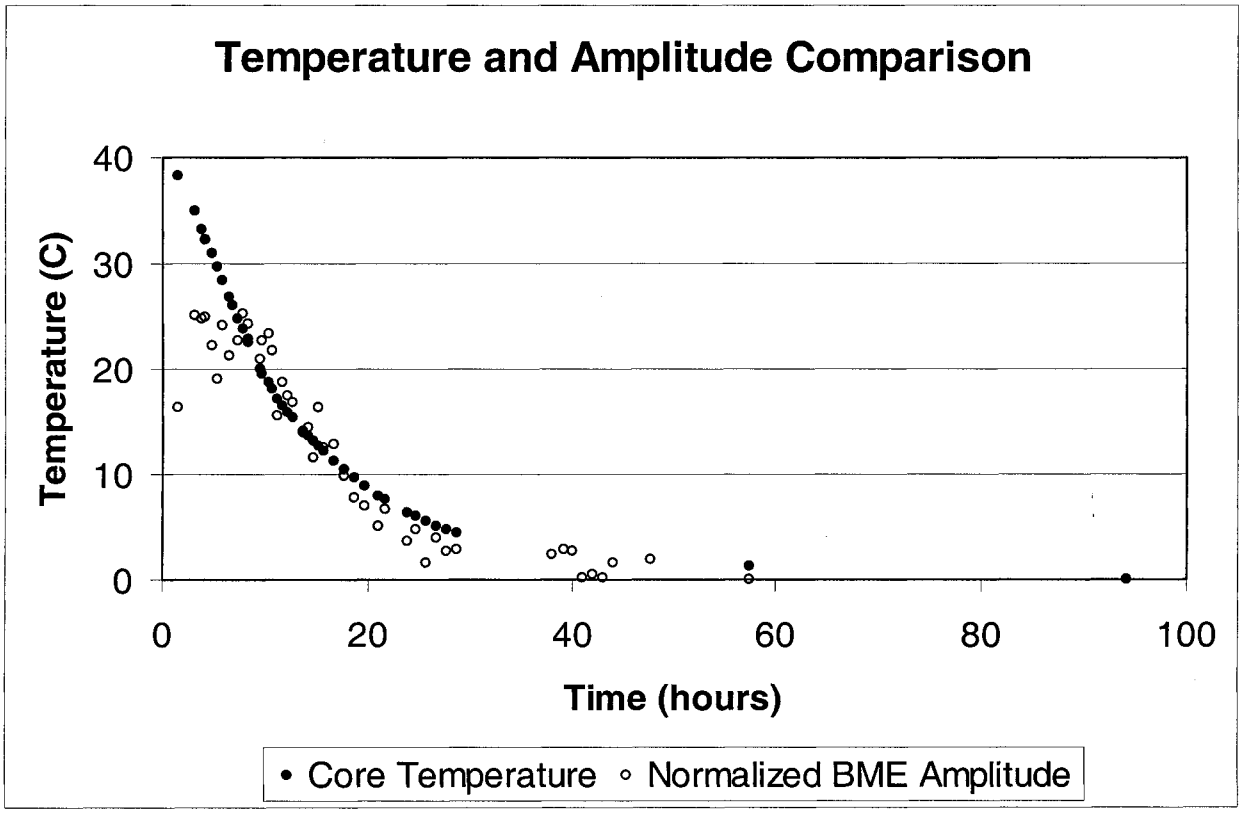

Figure 2-10 The decay comparison between the core temperature and normalized 900 MHz amplitude response.

4. ACKNOWLEDGMENTS

We would like to thank the following people and organizations that helped make this experiment a reality:

CSM Department of Geophysics- GPR equipment

Loveland Ski Patrol- Ron Kidder (patrol director) and Pip Baehler (assistant patrol director)

Cortemp technology HQ Inc.- Susan Smith

David Stillman, **Doug Klepacki**, and **Bruce Stott** for all the field work help!

5. REFERENCES

Achammer, T., and Denoth, A., 1994, Snow dielectric properties from DC to microwave X-band: Annals of Glaciol., v.19, p. 92-96.

Annan, A.P., September 2001, Ground Penetrating Radar Workshop Notes, Sensors & Software Inc., Mississauga, Ontario.

Appel 3rd, J. Z., Buhler, L., and Cooper, D. K., 2001, The pig as a source of cardiac xenografts: J. Card. Surg., v.16, n.5, p.345-356.

Balanis, C.A., 1989. Advanced Engineering Electromagnetics. New York: Wiley. 981p.

Duke, S.K., 1990, Calibration of ground penetrating radar and calculation of attenuation and dielectric permittivity versus depth: MSc Thesis, Dept. of Geophysics, Colorado School of Mines, Golden, 236 p.

Gabriel, C. and Gabriel, S., 1996, Compilation of the dielectric properties of body tissues at RF and microwave frequencies: Final Report AL/OE-TR-1996-0037, AFOSR/NL, Bolling AFB, Washington DC, var.pag.

Niessen, J., et al., 1994, The use of Ground Penetrating Radar to search for persons buried by avalanches: Proc.Fifth Int'l. Conf. Ground Penetrating Radar: Kitchener, Ontario, Canada, p.507-517.

Olhoeft, G. R., 1998, Electrical, magnetic, and geometric properties that determine ground penetrating radar performance: Proc. Seventh Int'l Conf. Ground Penetrating Radar: The University of Kansas, Lawrence, KS, USA, p. 177-182.

Olhoeft, G.R., 1988, Selected Bibliography on Ground Penetrating Radar, SAGEEP proceedings, p 462.

Powers, M. H., 1997, Modeling frequency-dependent GPR: The Leading Edge,16, no. 11, 1657-1662..

Shivola, A., 1999, Electromagnetic mixing formulas and applications: IEE, London, snow: p. 239-244.

Stern, W., 1929, Versuch einer elektrodynamischen Dickenmessung von Gletschereis: Ger. Beitr.zur Geophysik, v. 23, p 292-333.

Wolf, P., et al., 1997, The pig as a model in liver xenotransplantation: Vet. Res., v. 28, n.3, p. 217-222.

Yamaguchi, Y., Maruyama, Y., Kawakami, A., Sengoku, M., and Abe, T., 1991, Detection of objects buried in wet snowpack by an FM-CW radar: IEEE Trans. Geosci. Rem. Sens., v. 29, p.201-208.